Terrestrial Laser Scanning for Heliostat Surface Shape Determination and Canting Errors Correction

Maitane Ferreres Eceiza[1] [ID], Moritz Bitterling[1] [ID], Thomas Schmidt[1], William Baltus[2], Antoine Perez[2], Emmanuel Guillot[2] [ID], and Gregor Bern[1] [ID]

[1] Fraunhofer Institute for Solar Energy Systems ISE

[2] Processes, Materials and Solar Energy Laboratory, PROMES-CNRS

Abstract. Canting errors due to misalignments of heliostat facets pose a significant challenge to solar power plants' efficiency. Traditional methods of alignment are time-consuming and costly. This paper presents an innovative approach that employs Terrestrial Laser Scanning (TLS) technology for precise and fast heliostat alignment. The method involves point cloud processing, paraboloid fitting, and the adjustment of heliostat facet screws. A case study at the Thémis solar tower demonstrates the effectiveness, resulting in a significant improvement in optical quality and power output.

Keywords: Solar Field, Heliostats, Canting Errors, Terrestrial Laser Scanning, LiDAR

1. Introduction

Canting errors, i.e., inaccuracies in the pointing of a heliostat's facet caused by deviations of its two vertical and horizontal axes from the ideal orientation, lead to distorted flux distributions and increased spillage losses. Therefore, the efficiency of solar power plants can be significantly impeded by canting errors of heliostat mirrors. In recent research, canting errors have emerged as a critical concern in the operation of central receiver power plants, constituting one of the most prevalent challenges encountered [1]. Certain commercial plants have experienced increased slope and pointing errors in their heliostats, surpassing receiver specifications due to facet canting issues. These deviations lead to spillage losses that exceed initial projections and result in a performance decline within the field. A notable issue lies in the absence of specialized field tools within the industry to quantify these errors precisely and automatically during commissioning, hindering their timely rectification. Considering this, it becomes evident that there is a research gap for the advancement of precise tools capable of efficiently assessing and rectifying the canting of heliostats.

Presently, a variety of methods have been devised to address these challenges, both in terms of detection and correction. Traditionally, heliostat alignment was done by manual adjustment, utilizing the sun's reflection of single facets onto a target with the heliostat in tracking mode, or by means of gauge blocks or inclinometers [2]. Both techniques are time-consuming and costly, especially in large-scale solar power plants. Another approach is to use computer vision techniques to detect canting errors automatically. For example, some studies have used cameras to capture images of the heliostat surfaces, and then used image processing algorithms to detect misalignments from the known reflected structures [3]. Others use image processing algorithms to adjust the heliostats automatically based on their flux distribution [4]. However, these methods require special setups in the preassembly line, are sensitive

to lighting conditions, and may not be able to detect subtle misalignments. Additionally, these methods present difficulties in assigning the contribution of the flux map to individual facets.

Recent advances in terrestrial laser scanning (TLS) or light detection and ranging (Li-DAR) technology have enabled more precise and automated methods for heliostat alignment. In a previous study [5], LiDAR technology was used to capture the relative canting angles of artificially soiled heliostat mirror surfaces in 3D space, with the goal of automatically detecting canting errors by plane fitting. In this paper, we extend this approach by using terrestrial laser scanning to not only determine the canting angles, but also to correct them, validating its application for fast, systematic, and automated correction of heliostats canting in commercial power plants. Furthermore, we could show that a measurement without artificial soiling or temporary painting of reflector surfaces is possible when mirror cleanliness is less than 97% due to natural soiling.

2. Case study

The Thémis solar tower facility of PROMES-CNRS was chosen for the case study (see Fig. 1). The heliostat field of Thémis consists of approximately 201 heliostats arranged in a polar field, focusing on a central tower of 104 m height. The heliostats in the field have an aperture area of 54 m^2 and consist of nine modules each. Eight modules are distributed in two wings at either side of the heliostat pole, and a ninth smaller module is in between and above the pole. Each module consists of three vertical facets of parabolic mirrors and two facets in the smaller module. Each mirror strip is mechanically tightened to the module frame so that curvature and orientation are enforced. As a result, each module acts almost like a single parabolic facet, and the canting or orientation is controlled for each module independently, which is the focus of this study.

The canting of the heliostats was initially conducted during commissioning in the early '80s, and this study addresses the misalignments that have emerged since commissioning. The selected heliostat (Fig. 2) was experiencing significant spillage, motivating our investigation, to demonstrate the impact of canting errors on efficiency. By targeting a heliostat with noticeable spillage, we anticipated a substantial improvement in optical quality and power output after correction.

Figure 1. The Thémis solar plant of PROMES-CNRS in Targasonne (France). For one heliostat in the solar field, canting errors were quantified and rectified with terrestrial laser scanning, and the resulting change and improvement in the solar flux distribution at the flux target below the receiver was assessed.

Figure 2. *A Faro Focus S 70 laser scanner is used to capture a 3D point cloud of the front surface of heliostat E15 in the Thémis solar field. No additional artificial coating was applied to the heliostat mirrors, which had a cleanliness level due to natural soiling of between 93-97% for most of the mirror area.*

3. Methodology

3.1. Data capture and pre-processing

The TLS system used in this work (Faro Focus S 70) captures data sets consisting of three spatial coordinates, RGB values from a camera, and backscatter laser intensity. Natural soiling on mirror surfaces provides a dense point cloud without the need for additional coatings or markers. With a mirror cleanliness below 97%, point densities of 2000-10000 points/m^2 and above can be reached, leading to raw point clouds with sizes in the order of 100k to 1M points for one heliostat.

For automated pre-processing of the captured point cloud of a heliostat, the following steps were taken:

1) Remove points that are far from the central point of the cloud to eliminate points from the ground or neighboring heliostats.

2) Remove points with low brightness (based on their RGB value). This mainly eliminates points from the dark support structure.

3) Fit a plane to the remaining points to provide an initial transformation from the coordinate system of the measurement to the coordinate system of the heliostat.

3.2. Filtering and processing

Following the initial filtering and transformation, it is possible to fit a first estimate of the ideal paraboloid shape to the point cloud of the heliostat surface. The fit function, accounting for three translations, two rotations, and the curvature of the paraboloid, has six parameters. Fig. 3 shows the residuals of this fit. It is clearly visible that most of the statistical scattering of the points at the mirror surface is around ±1 cm. However, some points deviate further from the fitted paraboloid, up to 5 cm and more. The few points in front of the fitted paraboloid are from the mirror attachment brackets and screws (positive residuals), but most of the large residuals are in the back of the mirror (negative residuals)—they come from the mirror support structure. To prevent these points that are not from the reflector surface from skewing the fit results, points with residuals less than -2 cm (back) or greater than 3 cm (front) are removed from the point cloud.

The iterative process of refining the point cloud is crucial to ensure that only relevant data points contribute to the analysis. This filtering process minimizes the influence of extraneous elements, such as support structures and damaged areas, providing a clean dataset for subsequent analysis. Filters based on the center-of-mass and RGB values enhance the accuracy by isolating mirror surface points. However, due to reflections and structural elements, the residual-based filtering is essential for accurate surface assessment. Paraboloid fitting is introduced rather than plane fitting to account for curvature, significantly improving the accuracy of the surface fit. For a more detailed presentation of the paraboloid fit to a point cloud, see [6].

Using the same fit routine as above, the paraboloid fit is repeated with the cleaned point cloud to yield a refined estimate of the heliostat coordinate system, in which the pointing direction of the heliostat is exactly the z-axis. Knowing the design and the dimensions of the heliostat in this coordinate system, the point cloud can be automatically segmented into different groups corresponding to the nine heliostat modules. The points of each module are then fitted separately with planes, and the two angles of each plane's normal vector to the z-axis are calculated.
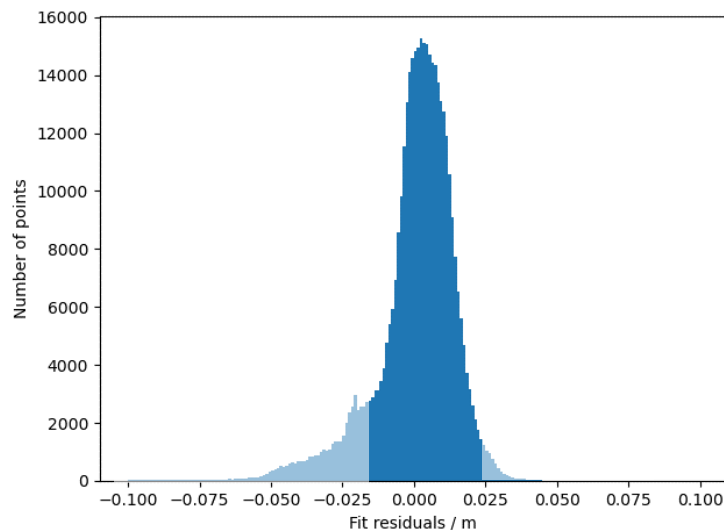

Figure 3. *Fit residuals of the first paraboloid fit of the point cloud of one heliostat. Negative residuals correspond to the back side of the reflector (mirror support structure), while positive residuals originate from the front (attachment brackets and screws). Based on this fit, a filtering of the point cloud is performed, discarding all points with large residuals indicated by the light blue region.*

4

4. Results and Discussion

In Fig. 4, the raw point cloud obtained with the scanner for the selected heliostat is shown. The first step is to perform an approximate transformation to the heliostat plane by detecting the edges. After the filtering around the center of mass and the visual brightness from RGB information of the camera is performed, most of the points corresponding to the support structure or to reflections are removed, as observed in Fig. 5.
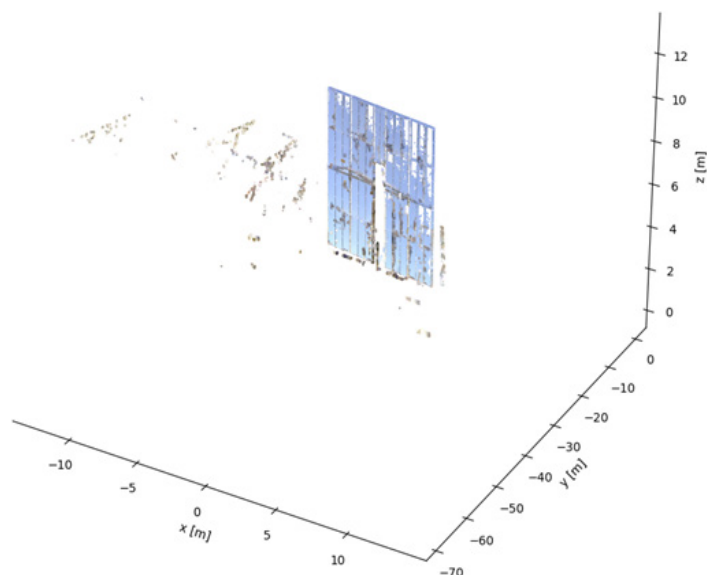

Figure 4. Raw measurement data for heliostat E15 from the laser scanner, without point cloud filtering and coordinate transformation.
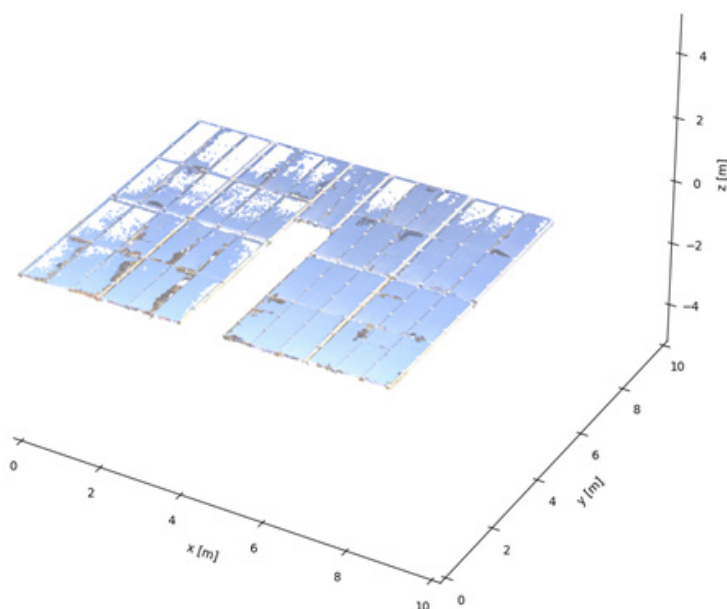

Figure 5. Pre-processed point cloud for the heliostat E15. Filtering was done based on RGB and spatial information, and the coordinate system was rotated to have the filtered point cloud coinciding with the xy-plane.

After the iterative paraboloid fitting process, the resulting paraboloid is shown in Fig. 6. With the iterative paraboloid fitting, the mean absolute deviation between the fit surface and the measurement points was reduced from 15 mm to less than 8 mm.
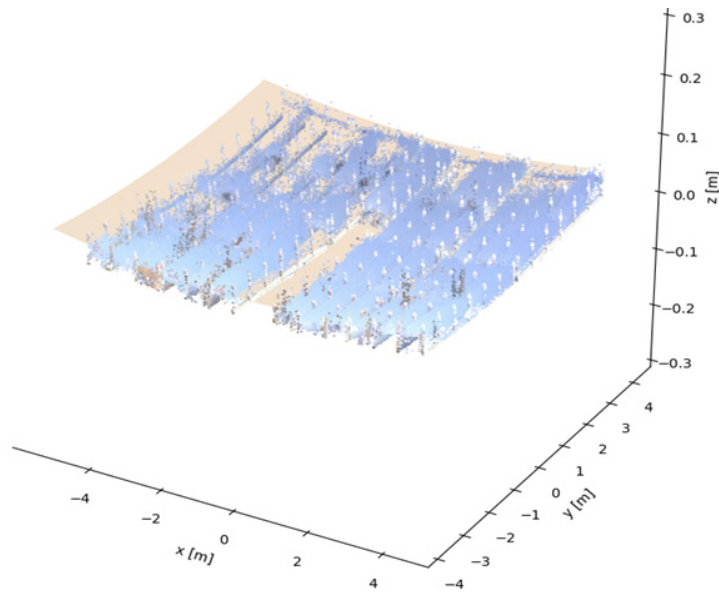
Figure 6. *Filtered point cloud for the heliostat surface (blue) and fit with an ideal paraboloid surface (orange). The parameters of the fit were used for a subsequent automatic segmentation of the point cloud into nine modules.*

From the filtered point cloud, the modules were selected, and a surface fitting was performed for each of them. The resulting direction of the normal vector of the facets can be seen in Fig. 7 (solid lines), where they are shown together with the theoretical normal vectors (dashed lines). For a paraboloid surface with a large focal length relative to its size, the surface normal vectors intersect at approximately twice the focal length from the surface (for a heliostat with the given dimensions and design focal length of 156 m, the error made with this approximation is less than 3 cm). For each of the modules, the two angular canting errors were derived from the difference between the fitted and ideal surface normal vectors. The uncertainty of the canting angles (obtained from the covariance matrix of the fit parameters) was between 0.03 mrad and 0.10 mrad depending on the module.
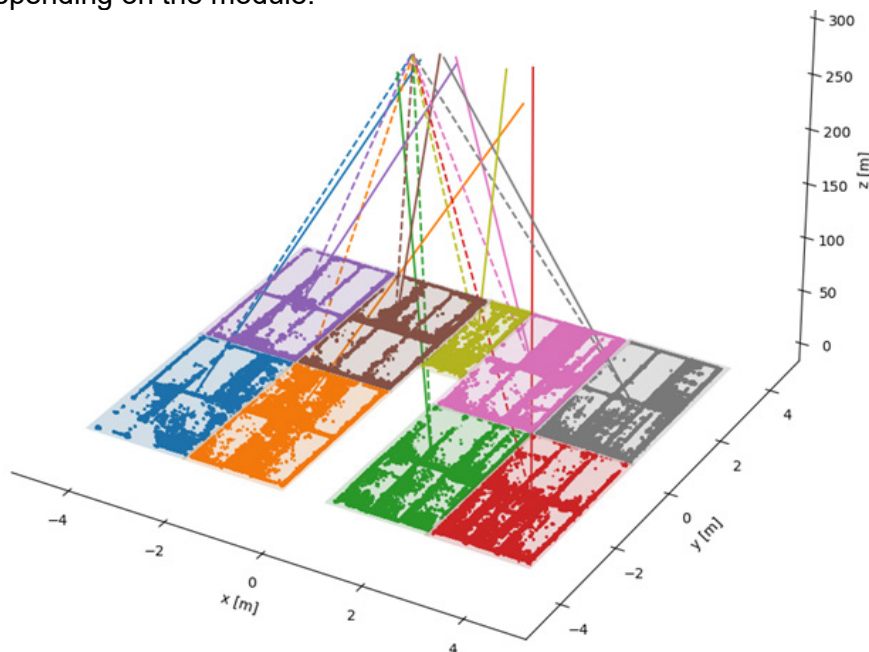

Figure 7. *Point cloud of the measured heliostat after segmentation into its nine separate modules. The points of each module were fitted with individual planes. The continuous lines show the direction of the normal vector for each fitted plane. The dashed lines show the corresponding ideal design normal vectors, which approximately intersect in the point 312 m from the heliostat. The deviation between continuous and dashed lines are the canting errors of the modules. Note the very compressed scale in z-direction compared to the xy-plane.*

6

Each module is supported on the heliostat structure in three points. By adjusting these three screw-nut assemblies, each module can be slightly tilted around the vertical and horizontal axes. With the known module sizes and the derived canting angles in the horizontal and vertical direction, the required direction and number of necessary screw-turns for correcting the canting were calculated. In Fig. 8, the calculated values for the three adjustment points for each module are shown.
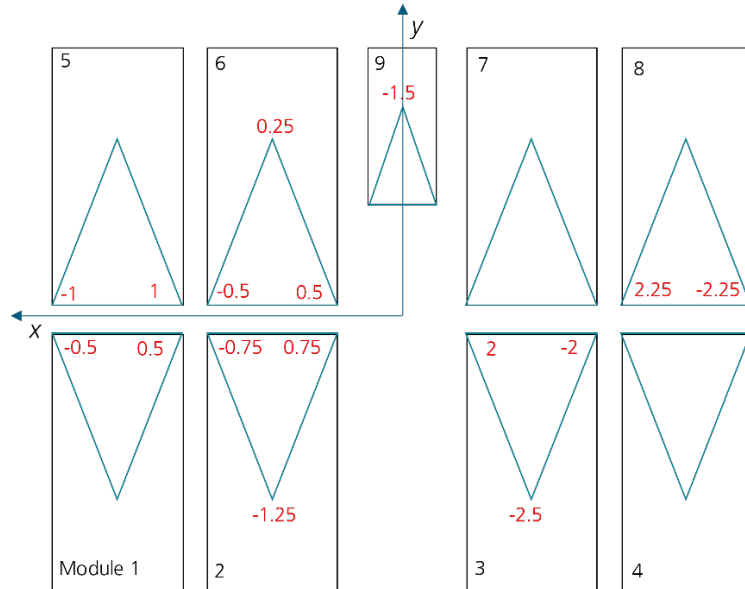
Figure 8. *Design of the heliostat and position of the canting adjustment screws for the nine modules (at the corners of the blue triangles). For each of the modules, the two angular canting errors were derived from the difference between the fitted and ideal surface normal vectors (Fig. 7). With the known module dimensions and the thread pitch of the 3 adjustment screws of each module, the required direction and number of screw turns were calculated (red) which are necessary to eliminate the canting errors.*

The calculated screw adjustments were supplied to the plant operator and maintenance team, and the corresponding predicted correction of the canting was directly applied to the heliostat. Flux measurements before and after correction (Fig. 9) demonstrate a doubling of maximum flux density (from 8 to 16 kW/m^2) and a 30% increase in thermal power output (23 to 30 kW in similar DNI and sun position conditions). The generated increased flux density and decrease in focal spot size highlights the high potential of the method for canting error measurement and correction.
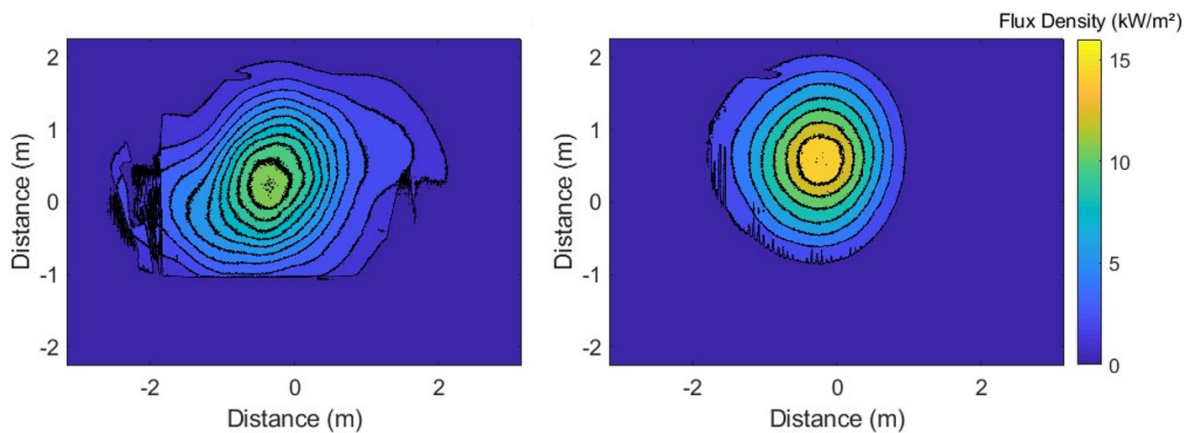
Figure 9. *Measured solar flux density at the target on the tower before (left) and after adjustment of the canting angles (right). At similar DNI, the integral power within the flux measurement area was increased from 23 to 30 kW, and the peak flux density from 8 to 16 kW/m^2. The estimated size of the focal spot was decreased from over 4x2 m^2 to less than 2x2 m^2 due to the heliostat improvement made, based on the laser scanning measurement.*

5. Conclusion and Outlook

The study demonstrates the feasibility of laser scanning for fast and accurate heliostat canting error correction. Even though the mean absolute error being around 8 mm, the large number of points measured on the naturally soiled mirror surface together with the filtering enables to obtain an uncertainty on the canting angles of 0.03 to 0.10 mrad. Therefore, TLS-based heliostat alignment proves to be a promising alternative to traditional approaches, offering great efficiency and accuracy. Future research should focus on further optimization and automatization of the process to maximize efficiency gains while exploring opportunities for broader industry adoption.

The integration of laser scanning into heliostat field measurements, such as during heliostat field commissioning or assessment, holds great potential for a fast and simultaneous assessment of cleanliness [7], canting and tracking. This represents a significant leap forward in the pursuit of solar field quality and efficiency.

Data availability statement

Data and supplementary material will be provided upon request.

Author contributions

M. Ferreres Eceiza and **M. Bitterling**: Conceptualization, Data curation, Formal analysis, Investigation, Methodology, Project administration, Software, Visualization, Writing – original draft. **T. Schmidt**: Conceptualization, Resources. **W. Baltus**: Investigation, Resources. **A. Perez**: Investigation, Resources. **E. Guillot**: Funding acquisition, Project administration, Supervision, Writing – review & editing. **G. Bern**: Conceptualization, Funding acquisition, Project administration, Writing – review & editing.

Competing interests

The authors declare that they have no competing interests.

Funding

References

[1] G. Zhu et al. Roadmap to Advance Heliostat Technologies for Concentrating Solar-Thermal Power. Golden, CO: National Renewable Energy Laboratory, 2022. https://doi.org/10.2172/1888029

[2] A. Sánchez-González, A. Lozano-Cancelas, R. Morales-Sánchez, J. C. Castillo, Canting heliostats with computer vision and theoretical imaging, Renewable Energy, v. 200, 2022, https://doi.org/10.1016/j.renene.2022.10.014

[3] J. Yellowhair, P. Apostolopoulos, D. Small, D. Novick, M. Mann. Development of an Aerial Imaging System for Heliostat Canting Assessments. SolarPACES 2020, AIP Conference Proceedings 2445, 12002, 2022. https://doi.org/10.1063/5.0087057

[4] A. Sánchez-González, B. Grange, C. Caliot. Computation of canting errors in heliostats by flux map fitting: experimental assessment. Optical Express, v. 28, n. 26, 2020. https://doi.org/10.1364/OE.412116

[5] C. Little, D. Small, J. Yellowhair. LiDAR for Heliostat Optical Error Assessment. SolarPACES 2020. AIP Conference Proceedings 2445, 120017, 2022. https://doi.org/10.1063/5.0087691

[6] M. Bitterling and M. Ferreres Eceiza, T. Schmidt, E. Guillot, G. Bern. Finding the Shape of the Largest Solar Furnace in the World. Presented at the 29th SolarPACES Conference in Sydney, Australia, October 10-13, 2023. https://doi.org/10.24406/publica-2839

[7] M. Ferreres Eceiza, M. Bitterling, T. Schmidt, T. Boehret, D. Wohlfeld, G. Bern. Terrestrial Laser Scanning for Fast Spatially Resolved Cleanliness Assessment of Heliostat Fields. SolarPACES Conference, 2022. https://doi.org/10.52825/solarpaces.v1i.705